Electrochemical Synthesis of Bismuth Iodide and Bismuth Oxyiodide

G. Mohan Kumar,[1,2] Deepak Suresh Varma[1,2], Sathiskumar Jothi[3,4], Devaraj Ramasamy[5], João C.C. Abrantes[5] and Murali Rangarajan[1,2,*]

[1]Center of Excellence in Advanced Materials and Green Technologies, Amrita School of Engineering Coimbatore, Amrita Vishwa Vidyapeetham, India

[2]Department of Chemical Engineering and Materials Science, Amrita School of Engineering Coimbatore, Amrita Vishwa Vidyapeetham, India

[3]Space 4.0 Limited, Aerospace Materials and Battery Development Division, England, UK

[4]Big Data Science & Technology Limited, Artificial Intelligence R&D Division, Greater London, England, UK

[5]proMetheus, Instituto Politécnico de Viana do Castelo, 4900-347 Viana do Castelo, Portugal

[*]Corresponding author email address: r_murali@cb.amrita.edu.

Abstract

This study reports the electrochemical synthesis of bismuth iodide and bismuth oxyiodide from acidic baths containing bismuth nitrate, sodium nitrate, iodine and ethylene glycol by a simple pH control. Linear sweep voltammetry analyses determined the potential window for the reduction of iodine where bismuth ion does not get reduced. The concentration of the iodide ions in the bath is regulated by the applied potential and the equilibrium that exists between iodine-iodide and nitrate-nitrite pairs. At pH 0.2 and 0.5, bismuth is predominantly present as free Bi^{3+} ions, which react with iodide to form bismuth triiodide. On the other hand, even at slightly elevated pH 1.0 and 2.0, bismuth is predominantly complexed by water, nitrates and ethylene glycol. These complexes react with the iodide ions to form bismuth oxyiodide. X-ray diffraction confirms that bismuth oxyiodide is predominantly formed at higher pH (1.0 and 2.0), while at lower pH (0.2 and 0.5), bismuth triiodide is formed. Impedance spectra are consistent with the above mechanism. The deposited bismuth oxyiodide films exhibit a cactus-like morphology formed from interlinked nano-disks, while the bismuth iodide films form micron-size platelet crystallites, both with good surface coverage. X-ray photoelectron spectroscopy confirms the formation of pure BiI_3 at pH 0.2, while binding energies of Bi 4f state in pure BiOI prepared at pH 2.0 has a slight shift towards higher binding energies. From diffuse reflectance spectroscopy studies, indirect bandgaps of electrochemically synthesized BiI_3 and BiOI were found to be 1.72 eV and 1.98 eV, respectively.

Keywords: bismuth iodide, bismuth oxyiodide, electrochemical synthesis, bismuth complexes, pH-dependent synthesis, X-ray diffraction.

Introduction

Bismuth iodides and oxyiodides have been subjects of many recent studies exploring applications such as radiation detection, digital imaging, photovoltaics and catalysis. They have been synthesized as polycrystalline powders, large single crystals or thin films. Among the early reports of synthesis of BiI_3 are studies from Singh *et al* [1] and Chaudhuri *et al* [2] who iodinated solution grown Bi_2S_3. Wang *et al* [3] synthesized BiI_3 by a hydrothermal protocol and explored their use for room-temperature X-ray detection. Studies have also been carried out on bismuth iodide synthesized using physical vapor deposition (typically involving a modified vertical Bridgman method) for X-ray detection and digital imaging [4-7]. Similar studies have also been carried out for radiation detection using BiI_3 [8], [9]. There has also been a significant interest in the exploration of BiI_3 as a photovoltaic material [10]. This is accomplished typically either by converting it into a methyl ammonium compound (see, for instance, [11]) and further doping it [12], or by preparing organic-inorganic hybrid systems [13] or by directly using it in an organic photovoltaic cell [10], [14]. The latter study uses a low-temperature solvothermal technique to prepare bismuth iodide. Recently, Wei *et al* [15] have used PVD-synthesized 2D layered nanoplates of BiI_3 for visible-light photodetection. Bismuth iodide has also been explored as catalysts for deprotection of acetals and ketals [16]. Finally, bismuth iodide nanowires have been obtained by calcination of a sonochemically-synthesized supramolecular precursor in a study by Soltanzadeh and Morsali [17].

Bismuth oxyiodides have also seen increasing interest among the research community particularly as environmentally safe photocatalysts in degrading organic and inorganic pollutants. Chang *et al* [18] have reported the photocatalytic degradation of sodium pentachlorophenate by chemically synthesized BiOI. Enhanced photocatalytic activity has been observed when these BiOI crystals have been modified by ionic liquids, for instance, 1-buty-3-methylimidazolium iodide, which are proposed to inhibit recombination of photo-

generated electrons and holes [19], [20]. Huang *et al* [21] have proposed a solvothermal method for defect engineering BiOI, such as introducing oxygen vacancies and IO_3^- doping into BiOI, which can minimise the photodegradation limitations of BiOI thereby enhancing their charge carrier dynamics and photocatalytic performance [22]. In addition to these reports, other approaches have been proposed for the synthesis of bismuth oxyiodide, including solvothermal/hydrothermal methods [23-26], chemical vapour transport using BiI_3 as starting material [27], microwave-assisted hydrothermal process [28], [29] and simple wet chemical synthesis [30-33]. In addition to photocatalytic effects, BiOI has been explored for photocurrent switching effect studies [28], [34], X-ray attenuation effect studies for medical imaging [30], antibacterial effect studies [32], and more recently, charge storage applications [35], suggesting BiOI as a potential material for wide range of applications.

Banik *et. al.* have reported [36] electrodeposition of BiI_3 on Au(111) substrates from electrolytes consisting of 50% ethanol. However, in our studies, we observe that bismuth iodide is significantly soluble in ethanol both in bulk and as thin films. To the best of the authors' knowledge, there have been no other reports of electrochemical synthesis of bismuth iodides. A few works have been published on electrochemical synthesis of bismuth oxyiodide, where aqueous solutions of $KBiI_4$ or $Bi(NO_3)_3$ with KI and benzoquinone have been used as electrolytes and the reduction of benzoquinone has been utilized to facilitate the hydrolysis of iodide [34], [37], [38]. In a recent work, galvanic deposition of BiOI has been achieved from a bath containing $Bi(NO_3)_3$, KI, $C_6H_4O_2$ and ethanol [39]. This work reports a simple electrochemical synthesis protocol for the preparation of bismuth iodide and bismuth oxyiodide thin films. Electrochemical synthesis has the advantage of excellent control over the driving force of the process even at ambient conditions. Along with a judiciously designed bath chemistry, it is possible to achieve fine control over the mechanism and rate of the synthesis. Thus, it is possible to synthesize a compound at ambient conditions and often achieve as good

purities as, say, solvothermal techniques at much shorter synthesis times. In this work, we choose an appropriate bath, containing bismuth nitrate and iodine, which establishes a controllable chemical equilibrium among the constituents. Then, by choosing appropriate deposition conditions such as the driving force (deposition potential), species concentrations in the bath and bath pH, we demonstrate that BiI_3 and BiOI thin films may be prepared. We also show that it is possible to control to an extent the stoichiometric ratio of BiI_x in the obtained films using suitable deposition conditions.

Experimental

The baths used in this study for electrochemical synthesis of bismuth iodide and bismuth oxyiodide comprise the following constituents: a source for Bi^{3+} ions, bismuth nitrate pentahydrate (Sigma Aldrich), elemental iodine (I_2) (Nice Chemicals), nitrate-containing supporting electrolyte, viz., sodium nitrate (Loba Chemie) and a suitable polyol. All chemicals used are of analytical grade. The bath pH is adjusted and fixed to predetermined values using 70% nitric acid. Graphite rod (Graphite India, GMMR-50) of 6 mm diameter was the working electrode, Ag/AgCl and 316 stainless steel were the reference and counter electrodes respectively. All electrodeposition (chronoamperometry) experiments were performed using Pine WaveNow (Pine Instruments, USA) potentiostat/galvanostat. Linear Sweep Voltammetry and electrochemical impedance spectroscopy were performed using CHI 604E (CH Instruments, USA) electrochemical workstation.

X–ray diffractograms were obtained using Rigaku X–ray diffractometer with X–rays from Cu target with 40 KV, 30 mA and K–beta filter. Rietveld refinements on XRD data were performed using the software TOPAS 5.0 (Bruker AXS, Karlsruhe, Germany) with the fundamental parameters approach. Field Emission Scanning Electron Microscopy (FESEM) characterization was performed using Carl Zeiss FESEM (SIGMA HV). X-ray Photoelectron

Spectroscopy (XPS) analysis was carried out using Kratos Axis Ultra machine. JASCO V 750 was used to record diffuse reflectance spectra.

Results and Discussion

Formation of BiI_3 and BiOI: Electrochemical deposition of bismuth triiodide/oxyiodide was explored in four different baths, all containing the same species at same concentrations, with the exception of bath pH, viz., 0.2, 0.5, 1.0 and 2.0. Figures 1 and 2 depicts the linear sweep voltammograms (LSV) of baths containing different combinations of the constituents, viz., Bi^{3+}, I_2, sodium nitrate and ethylene glycol at different pH values 0.2 and 2.0, respectively. The corresponding results for baths of pH 0.5 and 1.0 are presented in the Supporting Information (Figures S1 and S2, respectively). First, the peaks are assigned to the different reduction reactions that occur in the system. The LSV curves 1a and 1b (Figure 1 at pH 0.2) show strong reduction peak at 375-390 mV (vs. Ag/AgCl), that is absent in the curves 1c and 1d, the two of which (1c and 1d) have been obtained from baths without iodine. Similarly, the LSV curves 2a and 2b (Figure 2 at pH 2) show a strong reduction peak at 336-342 mV (vs. Ag/AgCl) that is absent in 2c and 2d, two of which (2c and 2d) are obtained without iodine in the bath. Similar reduction peaks are also observed in Figures 1e-f, 2e-f, corresponding to the baths containing iodine but no Bi^{3+} ions. Therefore, it may be concluded that this reduction corresponds to that of iodine. Comparing the LSV curves 1a-d and 2a-d with 1e-f and 2e-f reveals the reduction peak of bismuth in the curves 1a-d (−144 to −161 mV vs. Ag/AgCl) and 2a-d (−142 to −270 mV vs. Ag/AgCl), which are absent in 1e-f and 2e-f, respectively. The bath was regulated to a fixed value pH 0.2 (Figure 1) or pH 2 (Figure 2) by addition of nitric acid or sodium hydroxide. Therefore, even in Figures 1e-f and 2e-f, mild reduction peaks corresponding to nitrate reduction are observed. In fact, introducing $NaNO_3$ (especially at pH 2) substantially increases the peak reduction current, because both Bi^{3+} and NO_3^- reduce at near similar potentials (([40], [41]). These nitrate ions (either from the supporting electrolyte

$NaNO_3$ or HNO_3, added to maintain pH) allow for regulating iodine concentrations in the bath. Both water and ethylene glycol complex Bi^{3+} ions (further discussed below).

The key idea behind electrochemical synthesis of bismuth iodide compounds is to choose a bath containing Bi^{3+} ions and I_2 and reduce the latter without reducing the former. Figures 1a, 1b and 2a, 2b clearly show that iodine reduction to iodide occurs at more anodic potentials than Bi^{3+} reduction. Nitrate reduction is seen at potentials similar to that of Bi^{3+} [40-42]. Thus, there exists a potential window for reduction of I_2 without reducing Bi^{3+}. In this study, we have synthesized bismuth iodide and oxyiodide films under potentiostatic conditions where the deposition potential (for preparing BiI_3 or BiOI thin films) is fixed at +200 mV vs. Ag/AgCl RE (i.e., a cathodic polarization of –401 mV and –365 mV with respect to open circuit potential at pH 0.2 and 2.0, respectively).

Another interesting feature observed in the linear sweep voltammograms is the appearance of a second peak around iodine reduction in the presence of Bi^{3+} ions. Figures 1e-f and 2e-f, corresponding to 15 mM I_2 + 30% ethylene glycol and 15 mM I_2 + 30% ethylene glycol + 50 mM $NaNO_3$, do not show any visible second reduction peak around +300-400 mV (vs. Ag/AgCl). However, a second peak is clearly visible in Figures 1a-b, where 2 mM Bi^{3+} ions are added. In many non-aqueous and aprotic solvents and ionic liquids, iodine reduction is often observed as a two-step electrochemical process (see [43] and references therein), viz.,

$$3I_2 + 2e^- \rightleftarrows 2{I_3}^- \quad (1)$$

$${I_3}^- + 2e^- \rightleftarrows 3I^- \quad (2)$$

The first reaction, however, may actually be modelled [41] as

$$I_{2(aq)} + 2e^- \rightleftarrows 2{I^-}_{(aq)} \quad (3)$$

$$I_{2(aq)} + {I^-}_{(aq)} \rightleftarrows {I_3}^-_{(aq)} \quad (4)$$

The equilibrium constant for (3) has been reported [44] to be 698 M^{-1} in water. The introduction of Bi^{3+} ions results in a prominent second peak of triiodide formation, due to the conversion of iodide of bismuth iodide through a subsequent chemical reaction, given below.

$$Bi^{3+}{}_{(aq)} + 3I^{-}{}_{(aq)} \rightarrow BiI_{3(s)} \downarrow \qquad (5)$$

Finally, the iodine also forms protonated hypoiodous acid in aqueous solutions, given by

$$I_{2(aq)} + H_2O \rightleftarrows H_2OI^{+}{}_{(aq)} + I^{-}{}_{(aq)} \qquad (6)$$

with a forward rate constant of 0.12 s^{-1} an equilibrium constant 1.2×10^{-11} M in water [44]. Protonated hypoiodous acid, H_2OI^+, has a pKa of 1.4. Therefore, in the baths of pH 0.2, 0.5 and 1.0, this is the stable form of HOI.

To summarize, the electrolyte is expected to have four different iodine species, viz., I_2, I^-, I_3^- and H_2OI^+. However, under acidic conditions, such as the pH (0.2, 0.5, 1 and 2) studied in this work, Lengyel *et al*. [44] show that, in water, it is not the triiodide ions that are in large excess, but $[I_2] \gg [H_2OI^+] > [I^-] > [I_3{}^-]$, with the latter three species about four orders of magnitude less in amount than unreacted I_2. The additional electrochemical driving force available (–401 mV and –365 mV with respect to open circuit potential at pH 0.2 and 2.0, respectively, for potentiostatic deposition) substantially alters this concentration distribution within the boundary layer near the graphite electrode surface to $[I^-] > [I_2] > [I_3{}^-] > [H_2OI^+]$, primarily because electrochemical reduction of iodine is enabled.

When iodine is reduced to I^-, bismuth iodides of different stoichiometries could be synthesized. Since the electrochemical reduction of I_2 occurs at the cathode surface, the surface has higher concentration of iodide ions than the bulk, resulting in the diffusion of these ions in the interface towards the bulk. During this process, they encounter Bi^{3+} ions to form bismuth iodide, which then forms a film at the electrode surface. The consumption of Bi^{3+} ions will cause a counter-diffusion of Bi^{3+} ions towards the electrode surface, further accelerating the synthesis of the iodide.

Such a formation of bismuth iodide, through an irreversible chemical reduction process subsequent to an electrochemical reduction of iodine (an EC or EEC process, if iodine reduction is a two-step process), should render the former I_2 reduction more irreversible. In order to ascertain that the iodine reduction is a diffusion-controlled process, LSVs were performed at different scan rates from the bath with the presence of Bi^{3+} ions (Figure 3b) and the absence of Bi^{3+} ions (Figure 3a) at pH 0.2. Iodine reduction at the graphite electrode is diffusion-controlled, as evidenced by the square-root dependence of peak reduction current with scan rate, shown in Figure 3c and Figure 3d. However, Figure 3e-f shows that E_p has a weak dependence on the logarithm of scan rate, both in the presence and absence of Bi^{3+} ions. This is because the two steps in the reduction process are not resolved well. Similarly, LSVs and $i_{pc}\ vs\ \sqrt{\nu}, E_{pc}\ vs \log \nu$ relations for the bath with the presence of Bi^{3+} and absence of Bi^{3+} ions at pH 2 are depicted in Figures 4a-f. The corresponding results for pH 0.5 and 1.0 are reported in Figures S3 and S4, respectively.

The Bi^{3+} ions in the solution are present in the free or many aqua complexes (coordination number from 1 to 18; predominantly 6), [45-46], and coordination complexes with ethylene glycol [47-48]. Ethylene glycol, a Lewis base, is known to act as both monodentate and bidentate ligand, donating lone pairs of electrons to Bi^{3+} ions, exploiting their lone-pair distortion effects, thereby complexing them. Tooth [45] shows that the free Bi^{3+} ions are the dominant species at pH = 0.2, but at pH = 1.0 and above, it is the $[Bi_6(OH)_{12}]^{6+}$ complex that is the dominant species. This complex can be destabilized by the presence of I^- ions, which can displace six water molecules and in turn form oxyiodide compounds.

$$Bi_6(OH)_{12}{}^{6+} + 6I^- \rightarrow 6BiOI \downarrow + 6H_2O \qquad (8)$$

Indeed, at pH = 1.0 and 2.0, we observe the predominant formation of BiOI whereas at pH = 0.2 and 0.5, BiI_3 is the predominant species formed. McDonald and Choi [37] have also

observed that higher surface pH favours the formation of BiOI. Phase-pure BiI_3 and BiOI, were deposited in the same constituents' bath at pH 0.2 and 2, respectively. Characterization results obtained are discussed in the subsequent sections of this paper.

The presence of nitrate ions in the bath favours the establishment of a regulatory mechanism for controlling the concentration of iodide ions in the bath. This is well known and is often used in iodometric titrations to determine nitrate/nitrite concentrations.

$$NO_3{}^-{}_{(aq)} + 2H^+{}_{(aq)} + 2e^- \leftrightarrow NO_2{}^-{}_{(aq)} + H_2O \qquad (9)$$

$$NO_3{}^-{}_{(aq)} + 2H^+{}_{(aq)} + 2I^-{}_{(aq)} \leftrightarrow I_{2(aq)} + NO_2{}^-{}_{(aq)} + H_2O \qquad (10)$$

There is a recent report [49] and from our own lab results, bismuth iodide and oxyiodide may also be synthesized in bulk under ambient conditions by reacting a solution containing I_2/I^- ions with that containing Bi^{3+} ions. However, the solubility data of iodine [51] suggests that its feasibility is contingent on generating iodide ions in large quantities in bulk. In the present study, a controlled synthesis of iodide ions at an electrode surface provides for facile deposition of bismuth iodide thin films.

Electrochemical Impedance Spectroscopy: To further understand the processes of formation of these compounds, electrochemical impedance spectra were recorded at open circuit potential with amplitude ± 5 mV, over a frequency range of 0.01 Hz to 100 kHz. Experiments were conducted in an electrolyte containing 15 mM I_2 in 30% ethylene glycol solution in the presence and absence of 2 mM Bi^{3+} ions and 50 mM $NaNO_3$ at pH = 0.2 and 2.0, and the results are shown in Figure 5 as Nyquist plots. It is seen from Figure 5 that the effective charge transfer resistance for the formation of BiI_3 (pH = 0.2) is significantly higher than that of BiOI (pH = 2.0). A Gerischer-type impedance feature is observed in the medium to high frequencies, indicative of an EC mechanism (see inset of Figure 5) [52]. The low-frequency features reveal key differences between the two processes. At pH = 2.0, a low-frequency diffusion feature is observed, consistent with the diffusion of I^- ions generated at the surface towards the bismuth

complexes to facilitate the displacement of protons and the formation of BiOI films. Bismuth oxyiodide is known to have a tetragonal layered structure with each monolayer comprising slabs of $[Bi_2O_2]^{2+}$ sandwiched by slabs of I^- (see, for example, [53] and the crystal structure shown in Figure 7b). At pH = 2.0, Bi^{3+} is complexed by aqua, glycol and nitrates, mainly present as the hydrolysis complex $[Bi_6(OH)_{12}]^{6+}$ [45-48]. These complexes have the structure of protonated and hydrated bismuth oxides [53, 54]. Generation of I^- ions at the electrode surface may facilitate the deprotonation and dehydration of the hydrolysis complexes to form the layered oxyiodide structure. Their uptake of iodide to form bismuth oxyiodide is similar to various studies that have been carried out which have used different structural and morphological forms of bismuth oxides to selectively remove iodides from aqueous solutions. [53-55]. In these studies, starting from δ-Bi_2O_3, iodine chemisorption has resulted in the formation of the $Bi_4O_5I_2$ oxyiodide phase. Zhang et al [55] have shown that this uptake is best at pH between 1 to 3, room temperature and excess iodide present (up to 12:1 iodide : adsorbent ratio).

At pH = 0.2, a low-frequency semicircle with high magnitude of impedance is observed. This could be due to the trapping of free bismuth ions in the BiI_3 films [52]. As the pH increases, the concentration of free Bi^{3+} ions decreases, gradually eliminating such a phenomenon, thereby resulting in the decrease of low-frequency impedance (Figures 5).

Potentiostatic Deposition Films: Potentiostatic deposition studies were carried out to obtain thin films of bismuth iodide and oxyiodide from two baths. Sample A was electrodeposited from a bath prepared with 2 mM Bi^{3+}, 15 mM I_2, 50 mM $NaNO_3$ and 30% ethylene glycol at pH 0.2 and sample B corresponds to films electrodeposited from similar baths but at pH 2.0. Deposition was carried out at +200 mV (vs. Ag/AgCl) for 180 minutes. X-ray diffraction spectra were obtained for the thin films designated A and B. These results are depicted in Figure 6. At pH 2.0 (sample B), the obtained film is phase-pure BiOI, while, at pH 0.2 (sample A),

the obtained product is phase-pure BiI_3. These results are consistent with the electrochemical and interfacial chemical reactions that are expected to occur in these baths under the operating conditions. The availability of free Bi^{3+} ions favours the formation of bismuth iodide compound and the coordination complexations such as $Bi(OH)^{2+}$, $Bi_6(OH)_{12}^{6+}$ favours the formation of bismuth oxyiodide [44, 55-57]. The X-ray diffractograms of films deposited from baths of pH 0.5 and 1.0 are presented in Figure S5. The former contains predominantly BiI_3 with some BiOI, while the latter is comprised predominantly of BiOI with some BiI_3. Rietveld refinement was carried out for the X-ray diffractograms shown in Figure 6 and the details of the crystal structures obtained are depicted in Figure 7 and Table 1. These structures are consistent with pure phase BiI_3 and BiOI, respectively.

The morphologies of these thin films were examined using field emission scanning electron microscopy and all the films have substantial surface coverage. At pH 0.2, the representative surface morphologies of the BiI_3 films formed are shown in Figure 8 (a-d). Bismuth iodide forms as micron-sized polygonal (predominantly hexagonal) plates (of sizes 2.67 ± 0.63 µm, of thicknesses varying from 0.51 to 0.13 µm, measured using ImageJ software). These plates have grown in random directions. As seen in Figure 9 (a-d), sample B (prepared at pH 2.0) is predominantly BiOI which form as cactus-like flowers (of sizes 1.26 ± 0.29 µm, measured using ImageJ software), made of interlinked nano-size sheets (of thicknesses varying from 10 to 33 nm, measured using ImageJ software). FESEM of samples prepared at pH 0.5 (sample C, Figure S6 (a-d)) and pH 1.0 (sample D, Figure S7 (a-d)) are shown in the supporting information. The morphologies of these samples are similar to those of A and B. By visual examination, the intertwined nanoplates are further from each other.

X-ray Photoelectron Spectroscopy: X-ray photoelectron spectroscopy (XPS) analysis was carried out to ascertain the surface elemental composition of the electrodeposited BiI_3 and BiOI thin film samples. XPS is a surface sensitive analysis, hence, to avoid signals due to surface

oxidation (if there are any) interfering with BiI_3, XPS characterizations for samples A and C have been done at a depth of 10 nm after etching the film surface using Ar beam. From the survey spectrum (Figure 10 and Figure S8), the presence of Bi, I and O elements are observed in addition to carbon. High resolution Bi 4f (Figure 11a), doublet peaks of Bi $4f_{7/2}$ and Bi $4f_{5/2}$ are observed at binding energies 159 eV and 164.3 eV respectively corresponding to Bi^{3+} chemical state [58-60] of sample A, prepared at pH 0.2. This corresponds to the bismuth triiodide BiI_3, as also observed from XRD. In sample B (prepared at pH 2.0), there is a shift by 0.3 eV to higher binding energies 159.3 eV and 164.6 eV, corresponding to Bi $4f_{7/2}$ and Bi $4f_{5/2}$. This could be attributed to the oxidised phase of bismuth iodide that is bismuth oxyiodide. However, in both the samples, the binding energy difference between Bi $4f_{7/2}$ and Bi $4f_{5/2}$ is 5.3 eV, attributed to the trivalent vacancy states of Bi^{3+} ions in BiI_3 and BiOI, as should be the case [61]. High resolution spectra of I 3d chemical state (Figure 11b) has two peaks at 619.1 eV and 630.6 eV corresponding respectively to doublets of I $3d_{5/2}$ and I $3d_{3/2}$ of sample A and B. The energy difference between I $3d_{5/2}$ and I $3d_{3/2}$ is 11.5 eV, suggesting monovalent state of iodide [61] in both samples A and B. Both Bi 4f and I 3d states in sample A and B are symmetric suggesting that the sample A is a pure phase BiI_3 and sample B is a pure phase BiOI. Further to ascertain the oxidation state of the samples, high resolution O 1s spectra was obtained and presented in Figure 11c. From the HR O 1s spectrum of sample A, it is evident that the oxygen peak intensity is very weak compared with the intensities of Bi 4f and I 3d states. This indicates that the material formed is pure BiI_3. Further, the O 1s spectrum of sample B is fitted with three peaks at 530.1 eV, 531.5 eV and 532.8 eV. In the fitted peaks of sample B, the dominant peak at 530.1 eV is attributed to the lattice oxygen, Bi-O bonds in the $(Bi_2O_2)^{2+}$ slab of the material type BiOX [62]. The peaks at 531.5 eV and 532.8 eV are attributed to the hydroxyl group adsorbed on the surface of the film and the carbonyl (C-O) group respectively [63].

Optical Band Gap: In recent years, BiI_3 has been explored as absorber material in PV applications [10] due to its better optoelectronic properties and compatibility with the environment. Similarly, BiOI has been explored for photocatalytic applications using visible light [17-20]. Therefore, optical band gaps of the obtained films were studied using diffuse reflectance measurements. The reflectance spectra for the four films deposited are shown in Figure 12 (and Figure S9). The indirect band gaps of the BiI_3 and BiOI are obtained by plotting Kubelka-Munk function $(F(R)h\nu)^{1/2}$ vs $h\nu$ [64], are shown in Figure 13 (and Figure S10). Samples A and C (BiI_3) have band gaps of 1.72 and 1.7 eV, respectively, while samples B and D have band gaps between 1.98 and 1.85 eV, respectively, consistent with most reported values [60, 64]. Thus, both these films could be used for potential applications involving visible light.

Conclusions

This study presents a simple protocol for electrochemical synthesis of bismuth iodide and bismuth oxyiodide from aqueous acidic nitrate baths. Upon identifying the potential window for electroreduction of iodine but not Bi^{3+} ions, a simple control of bath pH enables selective synthesis of iodide vs. oxyiodide. Iodine is reduced in a controlled manner at the cathode surface to predominantly generate I^- ions. At a low pH of 0.2, free Bi^{3+} ions are the dominant species of bismuth in the bath, and these react with the electro-generated iodide ions to form bismuth triiodide (BiI_3). On the other hand, at a higher pH of 2.0, Bi^{3+} ions are predominantly complexed either by water or by ethylene glycol. These $Bi_6(OH)_{12}{}^{6+}$ complexes react with the electro-generated iodide ions to form bismuth oxyiodide (BiOI), even as some BiI_3 is also formed from the remaining free Bi^{3+} ions. Both BiI_3 and BiOI deposit as thin films on the cathode surface. Novel cactus-like morphologies of oxyiodide and hexagonal plates of iodide are obtained. These films have indirect band gaps of 1.98 and 1.72 eV, respectively.

Acknowledgments

The authors acknowledge financial support from Science and Engineering Research Board (SERB) through the core research grant (EMR/2017/000116), Ministry of Education through the FAST grant (F. No. 5-6/2013-TS.VII) and the Department of Science and Technology (DST) through the FIST grant (SR/FST/ETI-416/2016), for the conduct of this research.

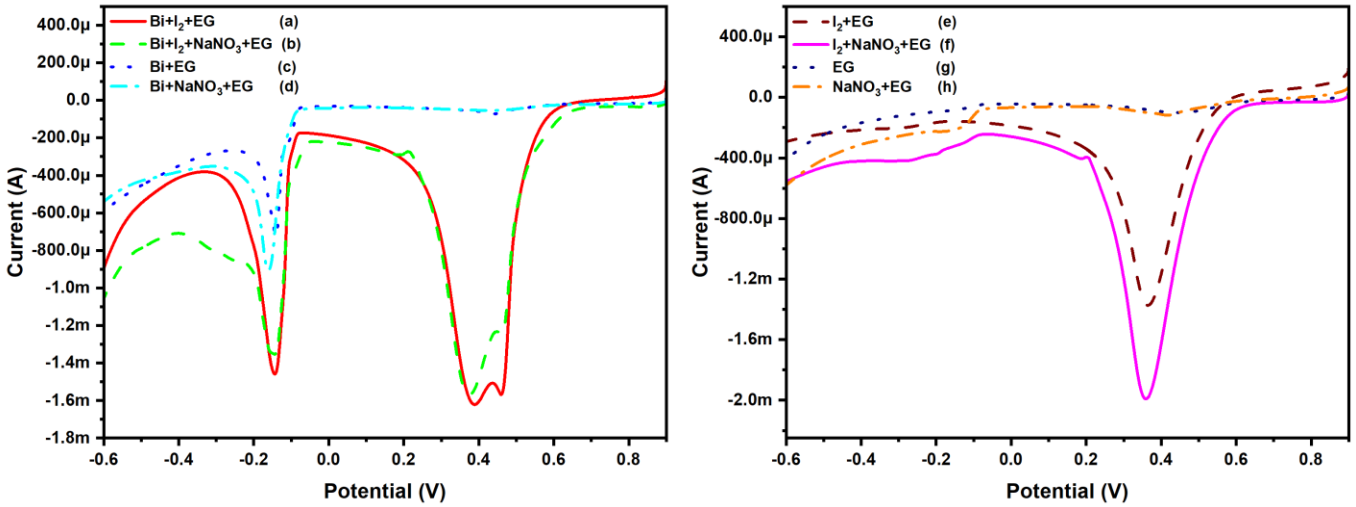

Figure 1. Linear sweep voltammograms of baths containing different combinations of the constituents viz., Bi^{3+}, I_2, $NaNO_3$ and ethylene glycol (EG) at $\nu = 50$ mV s^{-1}, pH 0.2.
a) Bi + I_2 + EG, b) Bi + I_2 + $NaNO_3$ + EG, c) Bi + EG, d) Bi + $NaNO_3$ + EG, e) I_2 + EG, f) I_2 +$NaNO_3$ + EG, g) EG and h) $NaNO_3$ + EG.

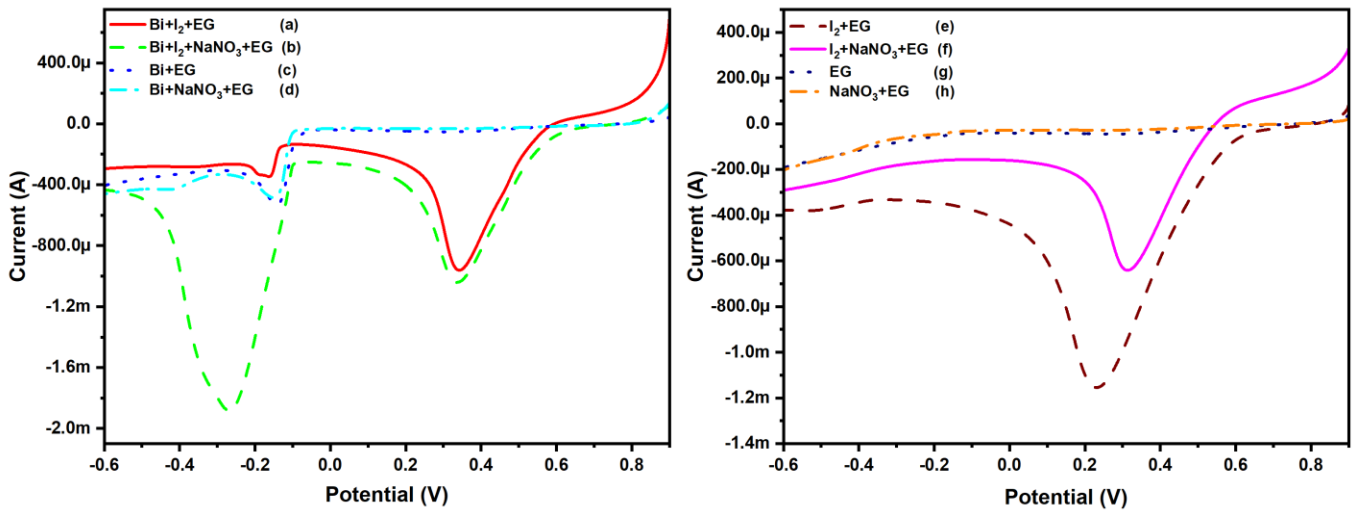

Figure 2. Linear sweep voltammograms of baths containing different combinations of the constituents viz., Bi^{3+}, I_2, $NaNO_3$ and ethylene glycol (EG) at $\nu = 50$ mV s^{-1}, pH 2.
a) Bi + I_2 + EG, b) Bi + I_2 + $NaNO_3$ + EG, c) Bi + EG, d) Bi + $NaNO_3$ + EG, e) I_2 + EG, f) I_2 +$NaNO_3$ + EG, g) EG and h) $NaNO_3$ + EG.

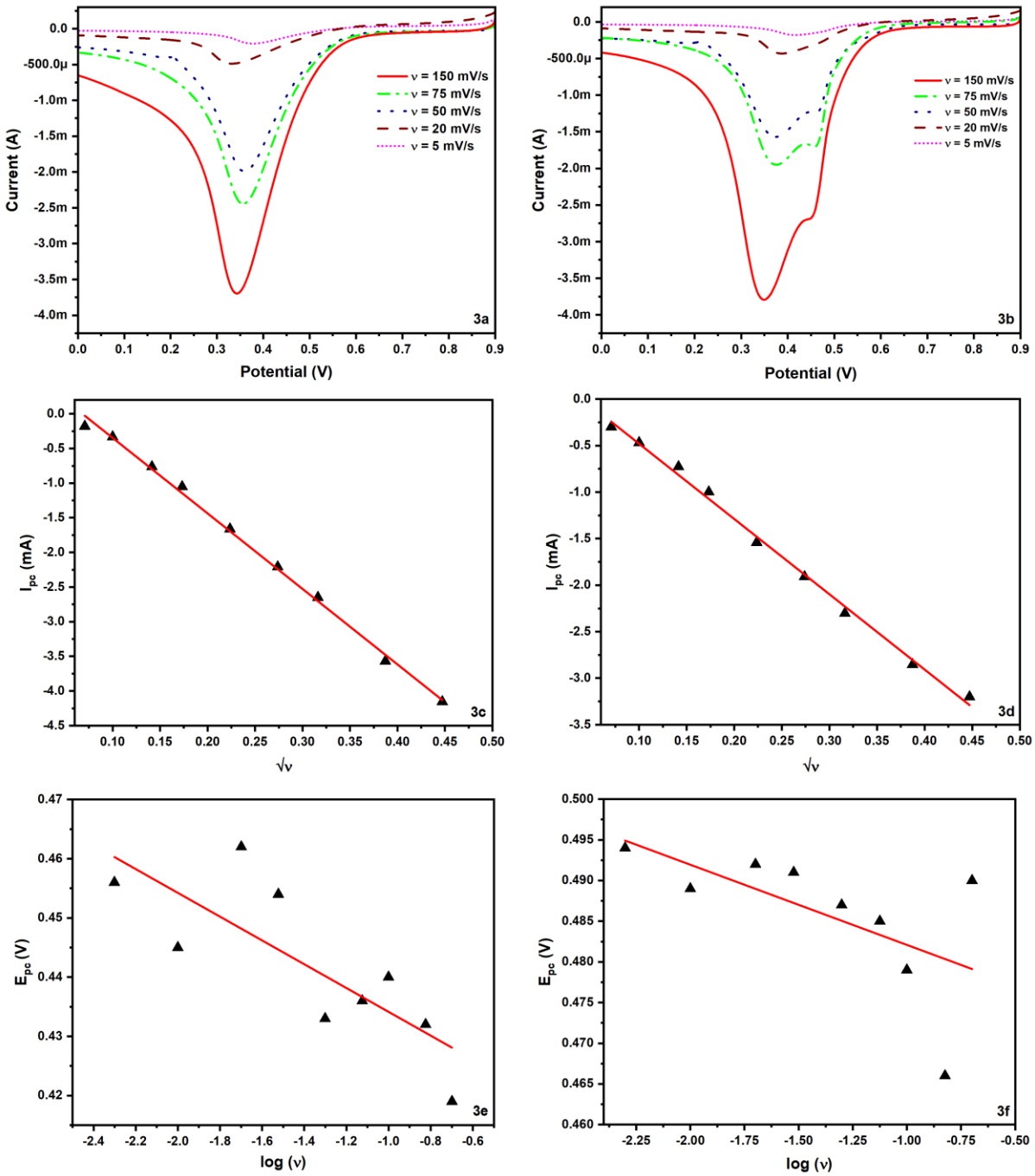

Figure 3a: LSV of iodine reduction for the different scan rates without Bi^{3+} ions, pH 0.2.

Figure 3b: LSV of iodine reduction for the different scan rates with Bi^{3+} ions, pH 0.2.

Figure 3c: Peak current vs. scan rate for iodine reduction without Bi^{3+} ions, pH 0.2.

Figure 3d: Peak current vs. scan rate for iodine reduction with Bi^{3+} ions, pH 0.2.

Figure 3e: Peak potential vs. log (scan rate) for iodine reduction without Bi^{3+} ions, pH 0.2.

Figure 3f: Peak potential vs. log (scan rate) for iodine reduction with Bi^{3+} ions, pH 0.2.

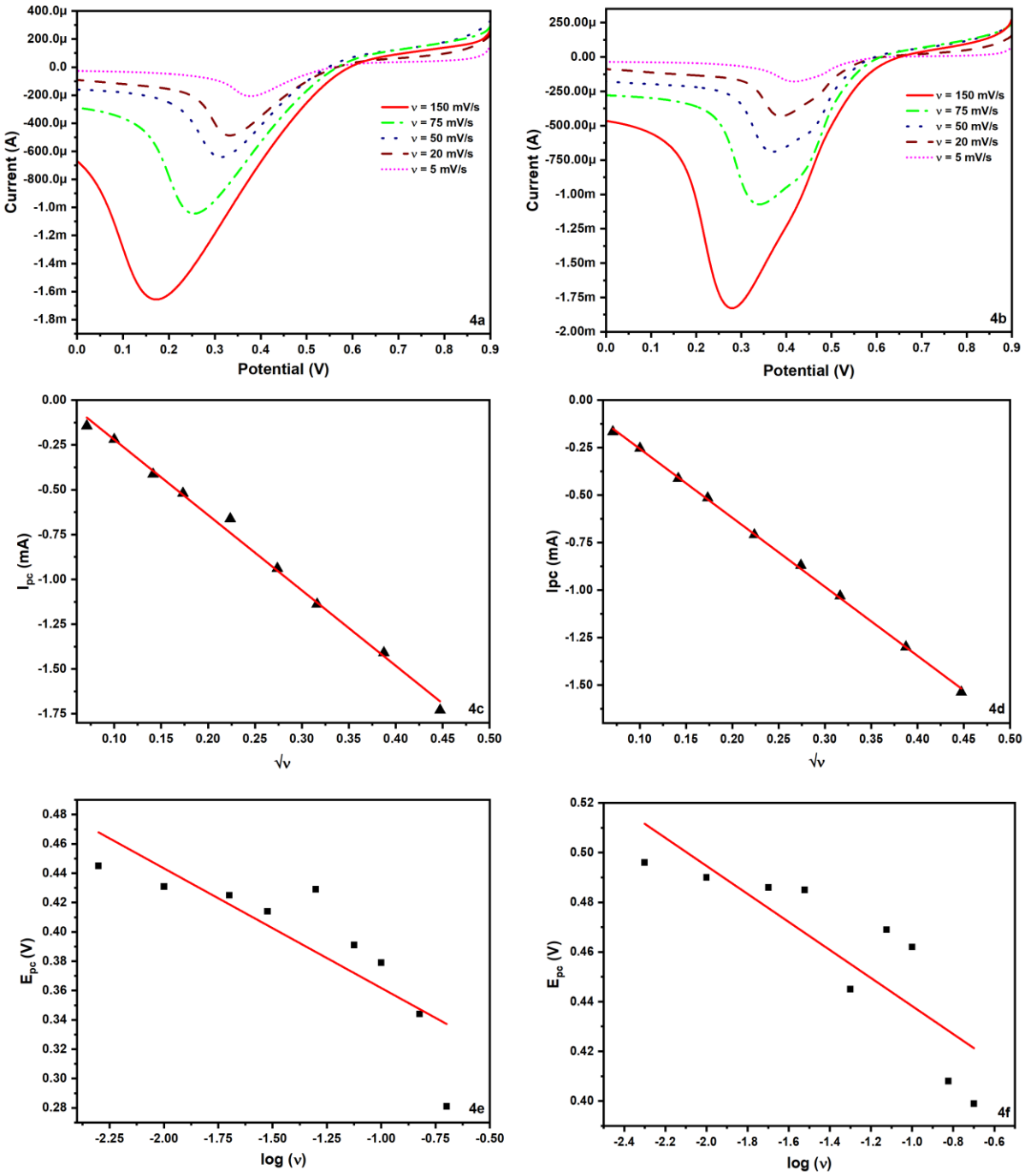

Figure 4a: LSV of iodine reduction for the different scan rates without Bi^{3+} ions, pH 2.

Figure 4b: LSV of iodine reduction for the different scan rates with Bi^{3+} ions, pH 2.

Figure 4c: Peak current vs. scan rate for iodine reduction without Bi^{3+} ions, pH 2.

Figure 4d: Peak current vs. scan rate for iodine reduction with Bi^{3+} ions, pH 2.

Figure 4e: Peak potential vs. log (scan rate) for iodine reduction without Bi^{3+} ions, pH 2.

Figure 4f: Peak potential vs. log (scan rate) for iodine reduction with Bi^{3+} ions, pH 2.

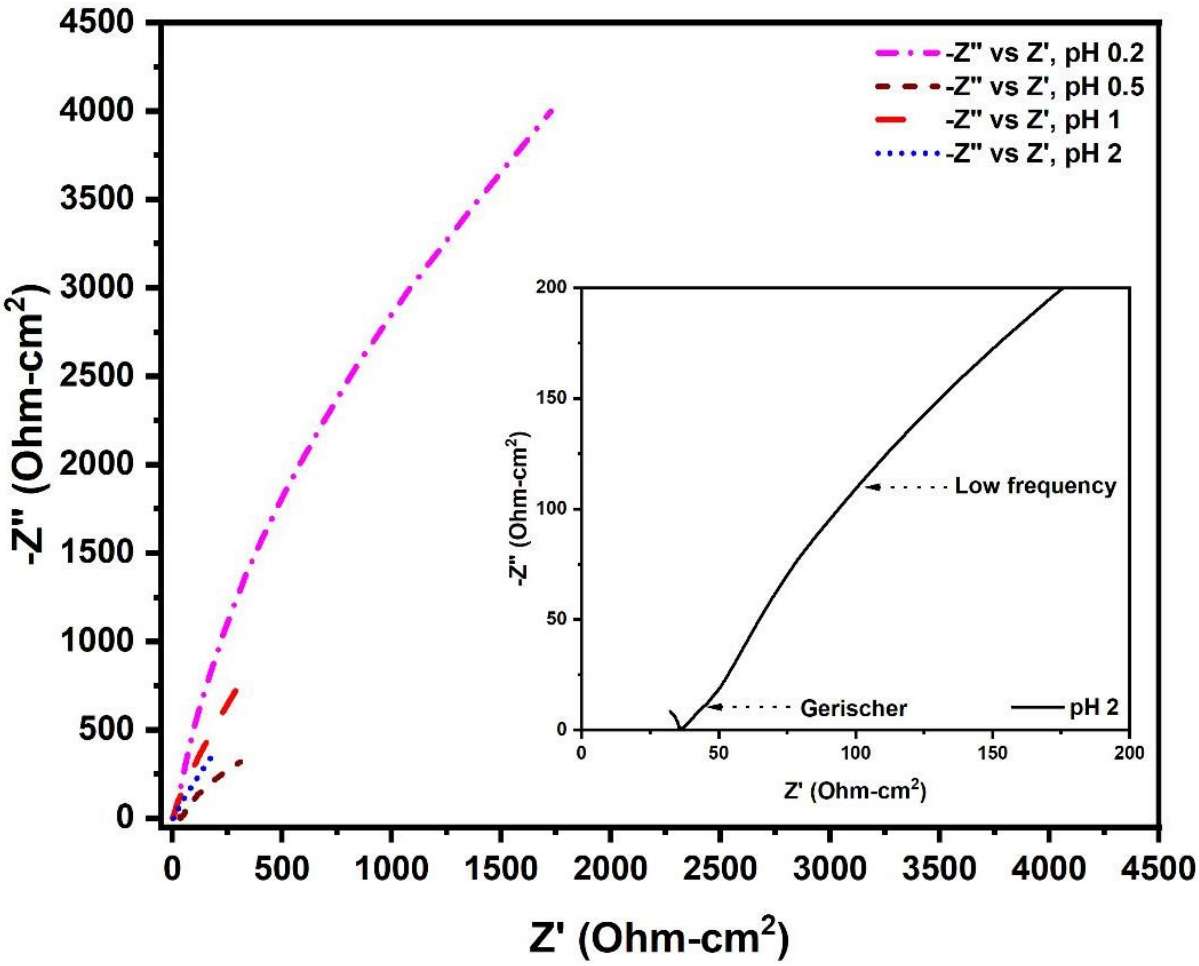

Figure 5. Electrochemical impedance spectra (Nyquist plots) depicting $-Z'' \; vs. \; Z'$ for all four pH of the bath studied (0.2, 0.5, 1.0, 2.0); EIS recorded at OCP ±5 mV, frequencies ranging from 0.01 Hz to 100 kHz.

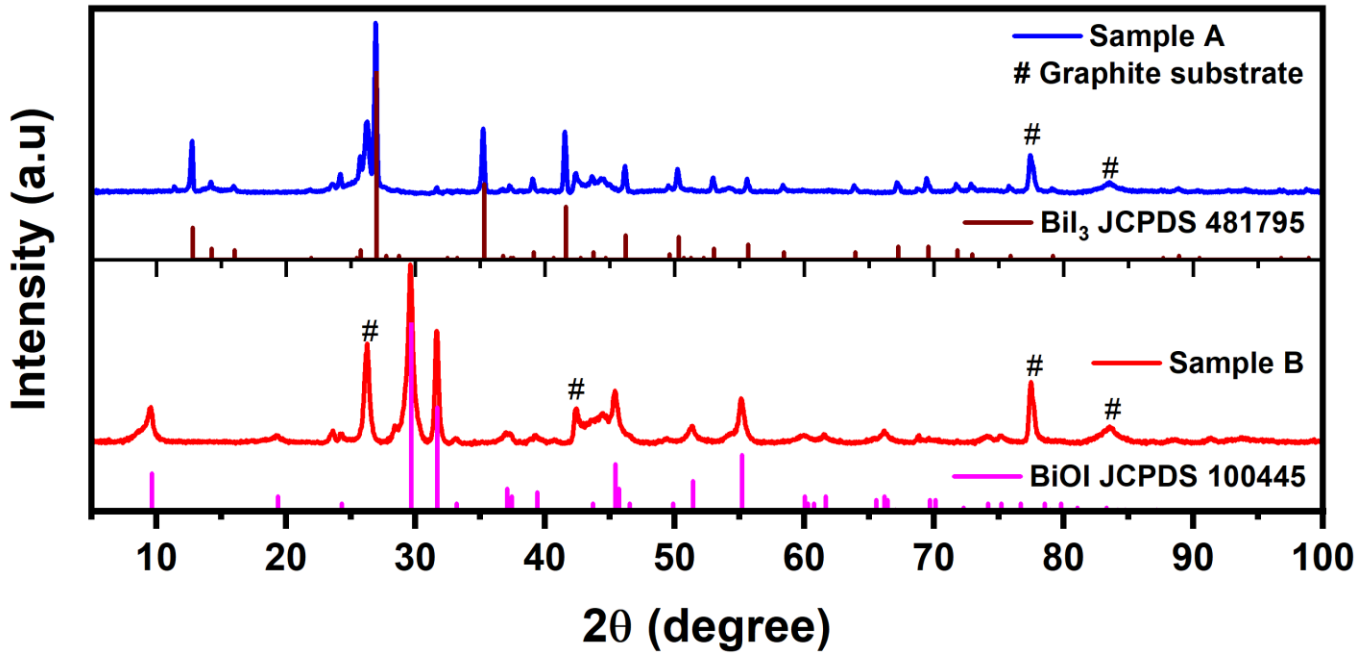

Figure 6. X ray diffraction patterns of electrodeposited BiI_3 (Sample A) and BiOI (Sample B) thin films on graphite substrate; Deposition potential: +200 mV vs. Ag/AgCl RE; For BiI_3, bath pH is 0.2 and for BiOI, bath pH is 2.0.

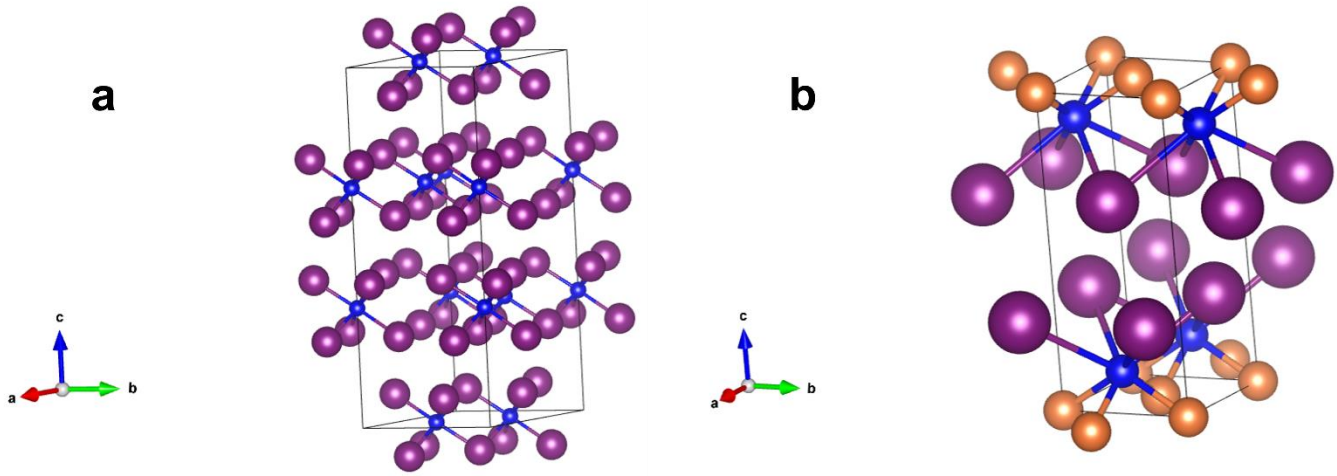

Figure 7. Crystal Structures of Electrodeposited Phase-Pure Species. (a) BiI_3, obtained from baths at pH 0.2, (b) BiOI, obtained from baths at pH 2.0.

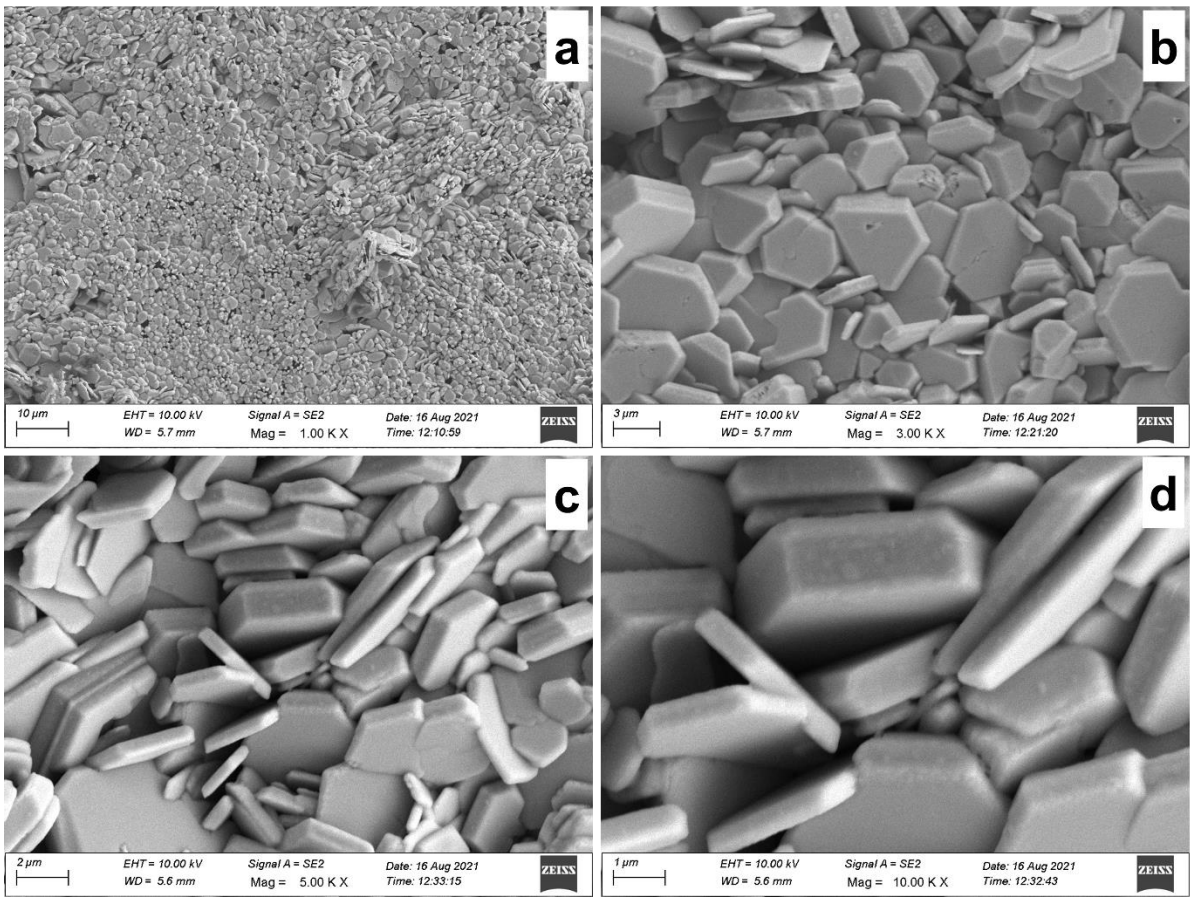

Figure 8 (a-d). FESEM morphologies of electrodeposited BiI_3 (sample A); Deposition conditions: Bath prepared from 2 mM Bi^{3+}, 15 mM I_2, 50 mM $NaNO_3$, 30% ethylene glycol, pH 0.2, at 200 mV (vs. Ag/AgCl).

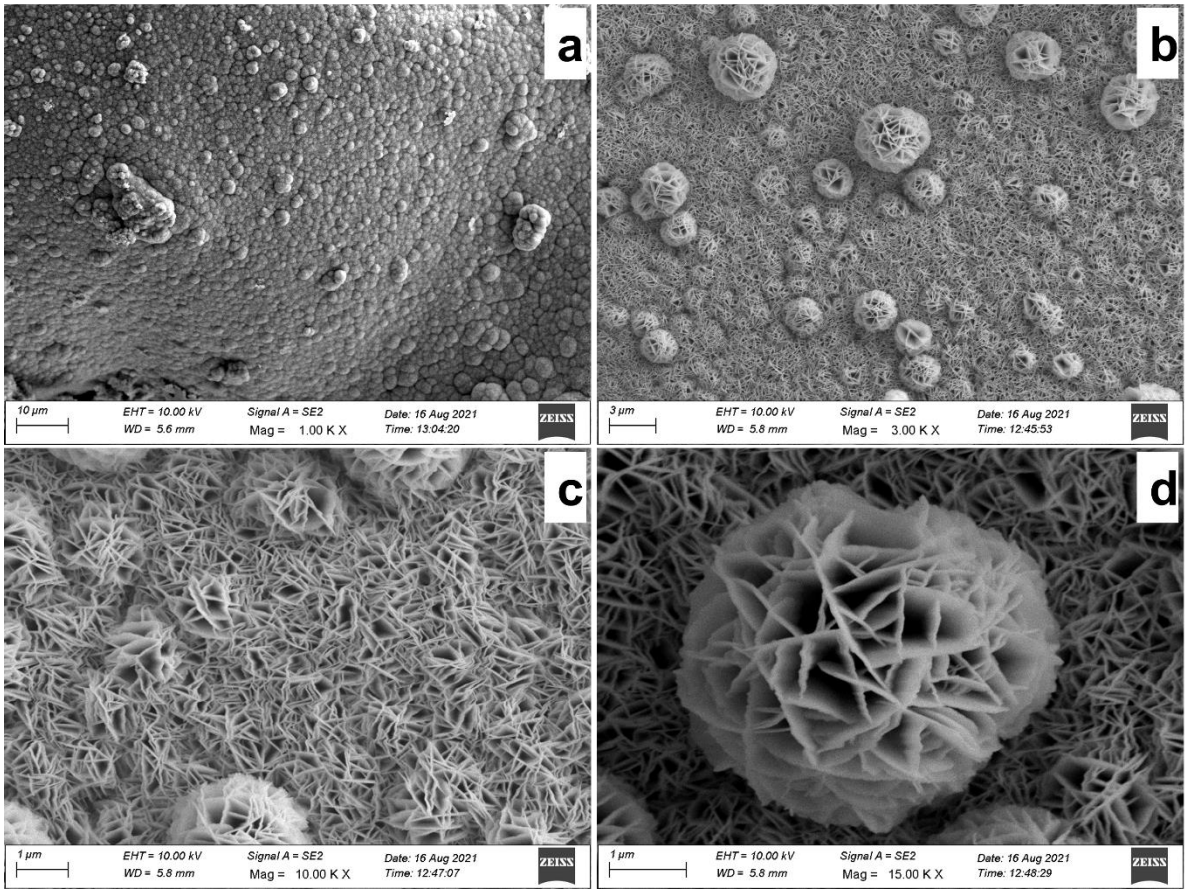

Figure 9 (a-d). FESEM morphologies of electrodeposited BiOI (sample B); Deposition conditions: Bath prepared from 2 mM Bi^{3+}, 15 mM I_2, 50 mM $NaNO_3$, 30% ethylene glycol, pH 2.0, at 200 mV (vs. Ag/AgCl).

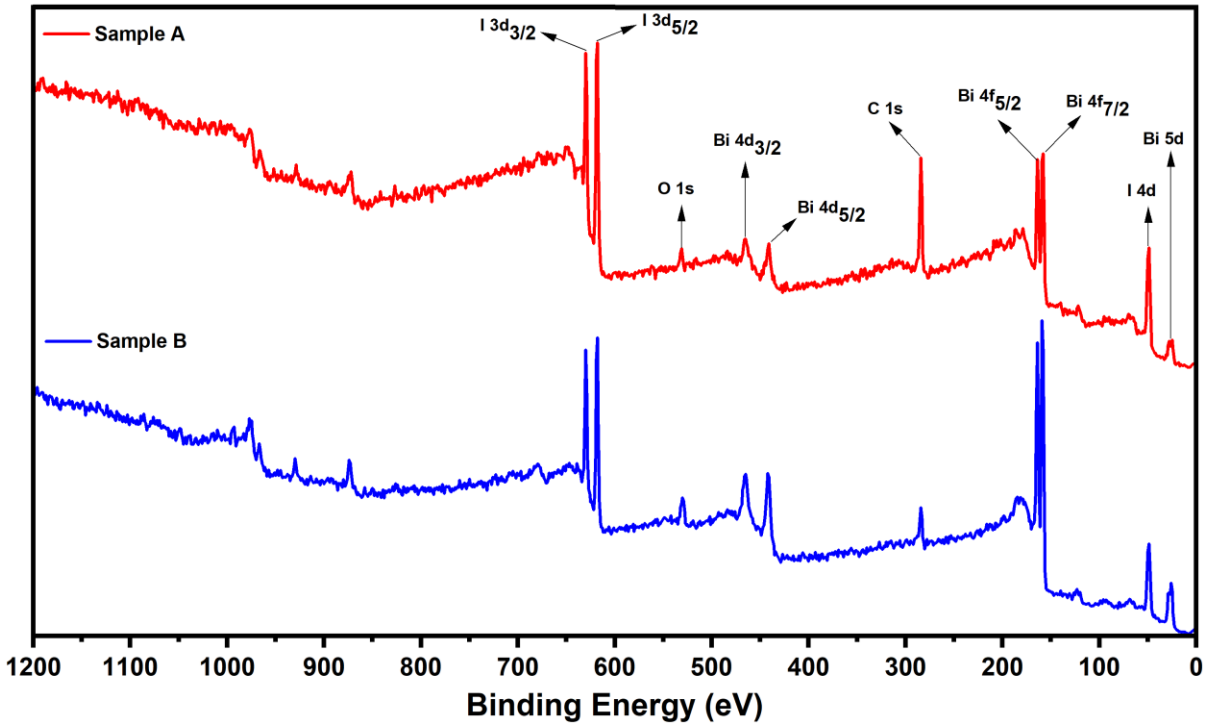

Figure 10. X ray photoelectron spectroscopy (survey spectra) of samples A (pH 0.2) and B (pH 2.0) (Deposition conditions are listed in the captions of Figures 8 and 9.)

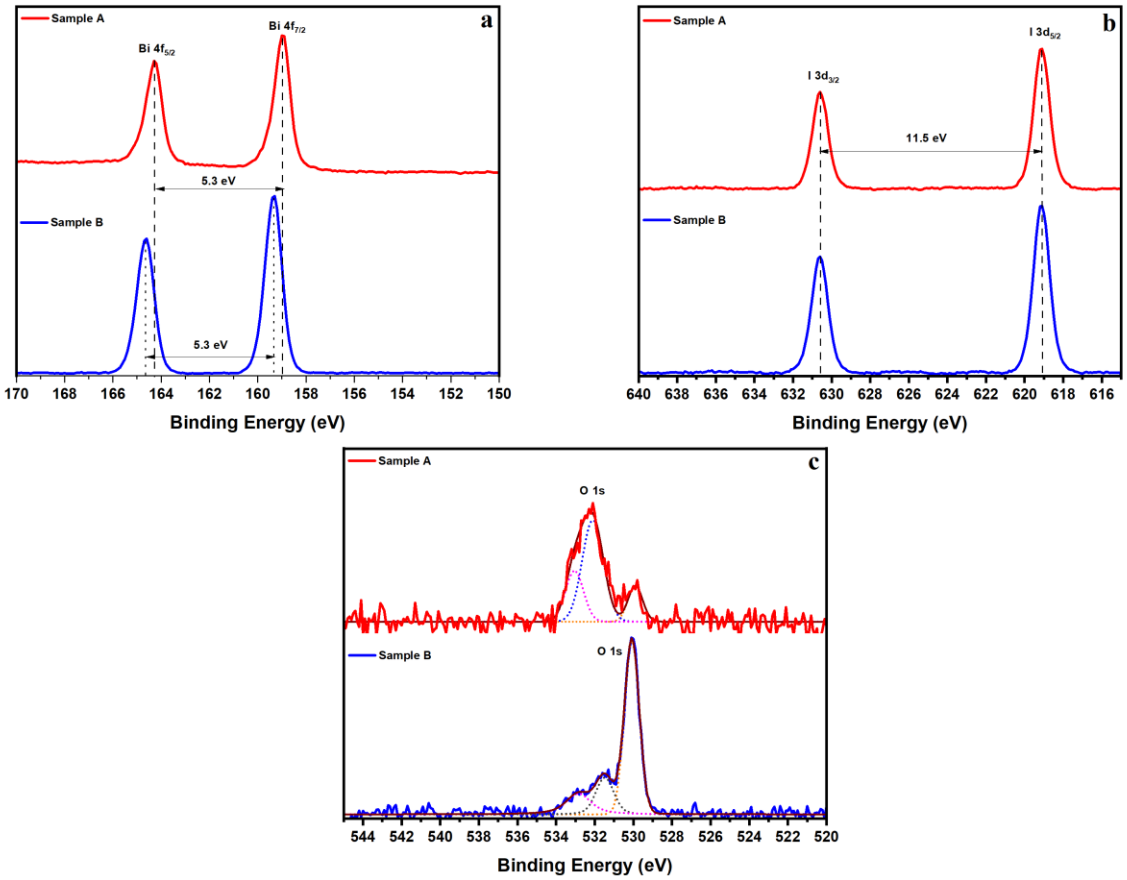

Figure 11. High resolution XPS of samples A (pH 0.2) and B (pH 2.0), a) Bi 4f, b) I 3d and c) O 1s states. (Deposition conditions are listed in the captions of Figures 8 and 9).

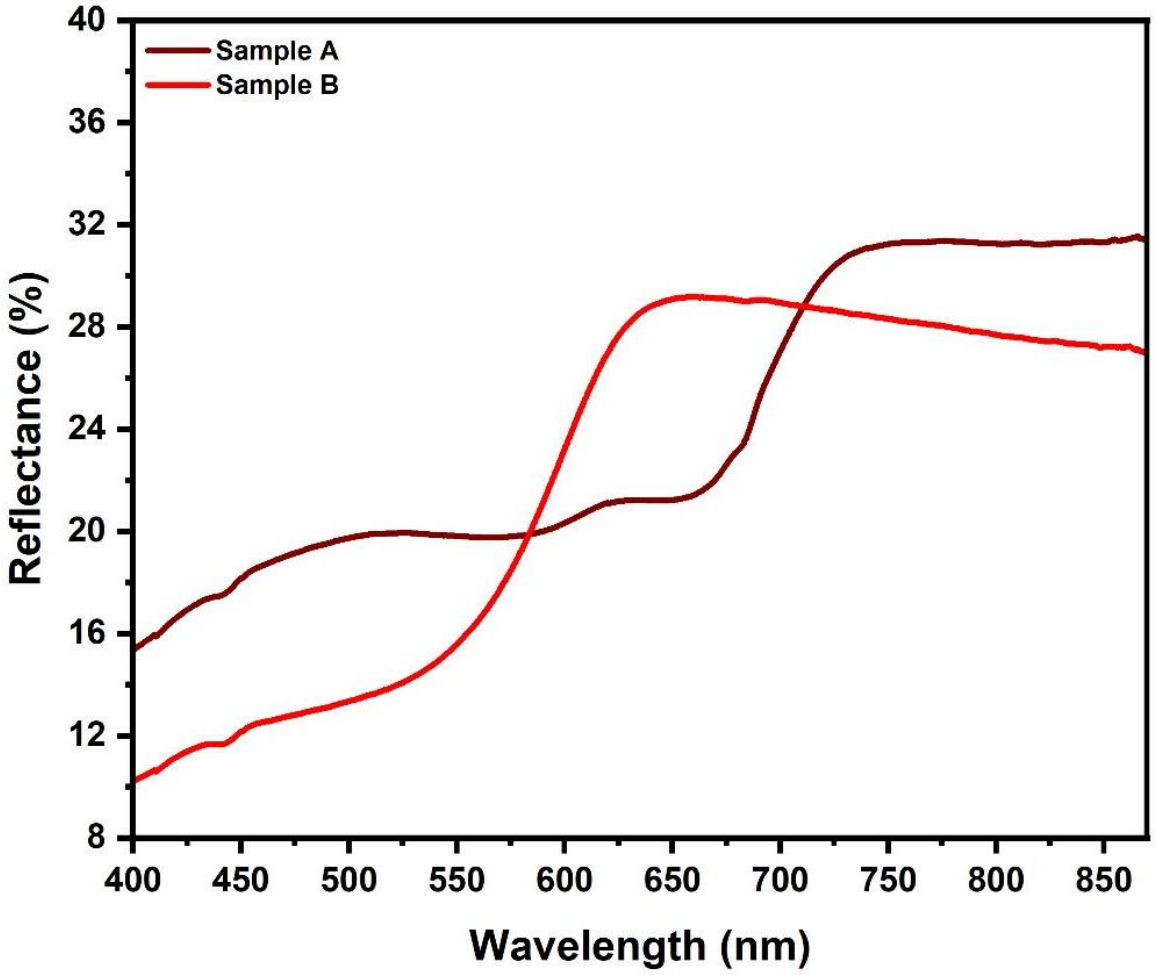

Figure 12. Diffuse reflectance spectra of electrodeposited BiI_3 and BiOI, sample A (prepared at pH 0.2), sample B (prepared at pH 2), sample C (prepared at pH 0.5) and sample D (prepared at pH 1).

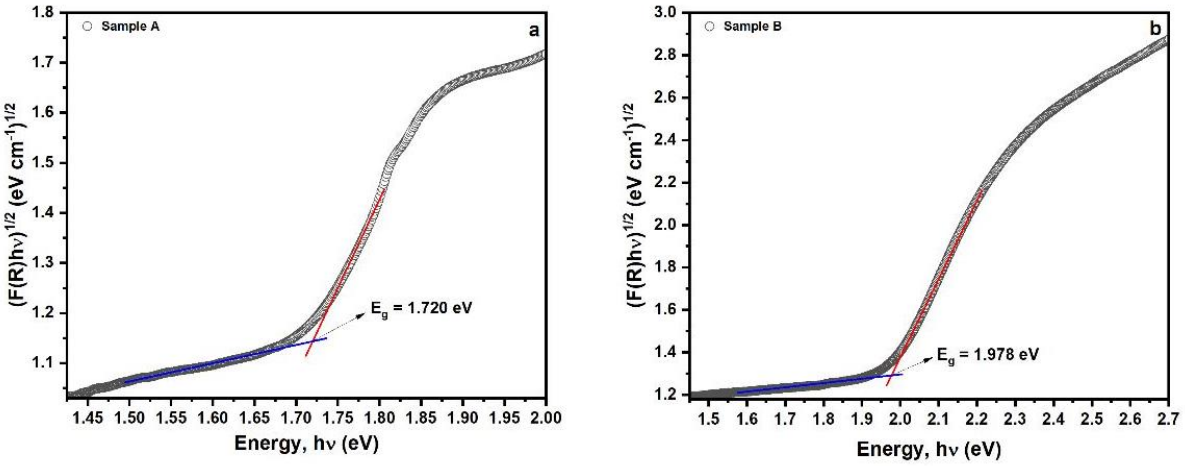

Figure 13. Kubelka-Munk function, $(F(R)h\nu)^{1/2}$ vs hν plot to determine the optical bandgap (indirect transition) of electrodeposited BiI_3 and BiOI, sample A (prepared at pH 0.2), sample B (prepared at pH 2).

Table 1. Crystal parameters for electrodeposited phase-pure BiI_3 and BiOI on graphite substrate

Phase	Bismuth Iodide, BiI_3	Bismuth Oxyiodide, BiOI
Space Group	$R\bar{3}$	P4/nmm
Crystal system	Trigonal	Tetragonal
Lattice system	Rhombohedral	Tetragonal
Lattice Parameters		
a = b (Å)	7.517	3.994
c (Å)	20.713	9.149
$\alpha = \beta$	90°	90°
γ	120°	90°
c/a	2.756	2.291

References

1. S.K. Singh, B.B. Nayak, B. S. Acharya and B. C. Mohanty, *React. Solids.,* **4,** 173 (1987).

2. T. K. Chaudhuri, A. B. Patra, P. K. Basu, R. S. Saraswat and H. N. Acharya, *Mater. Lett.,* **8**, 361 (1989).

3. C. Wang, Q. Yang, K. Tang, and Y. Qian, *Chem. Lett.,* **30**, 154 (2001).

4. A. Cuña, I. Aguiar, A. Gancharov, M. Pérez, and L. Fornaro, *Cryst. Res.Technol.,* **39**, 899 (2004).

5. L. Fornaro, A. Cuna, A. Noguera, M. Perez, and L. Mussio, *IEEE Trans. Nucl. Sci.,* **51,** 2461 (2004).

6. I. Aguiar and L. Fornaro, *Scientia Plena*, **4** (2008).

7. I. Aguiar, A. Olivera, M. Mombrú, H. B. Pereira and L. Fornaro, *J. Cryst. Growth*, **457**, 244 (2017).

8. A. T. Lintereur, W. Qiu, J. C. Nino and J. Baciak, *Nucl. Instrum. Methods Phys. Res. A*, **652**, 166 (2011).

9. S. S. Gokhale, H. Han, J. E. Baciak, J. C. Nino and K. A. Jordan, *Radiat. Meas.,* **74**, 47 (2015).

10. D. Tiwari, D. Alibhai and D. J. Fermin, *ACS Energy Lett*. **3**, 1882 (2018).

11. R. L. Z. Hoye, R. E. Brandt, A. Osherov, V. Stevanovic, S. D. Stranks, M. W. B. Wilson, H. Kim, A. J. Akey, J. D. Perkins, R. C. Kurchin, J. R. Poindexter, E. N. Wang, M. G. Bawendi, V. Bulovic and T. Buonassisi, *Chem. Eur. J.*, **22**, 2605 (2016).

12. M. Vigneshwaran, T. Ohta, S. Iikubo, G. Kapil, T. Ripolles, Y. Ogomi, T. Ma, S. S. Pandey, Q. Shen, T. Toyoda, K. Yoshino, T. Minemoto, and S. Hayase, *Chem. Mater.,* **28**, 6436 (2016).

13. D. M. Fabian and S. Ardo, *J. Mater. Chem. A*, **4**, 6436 (2016).

14. K. M. Boopathi, S. Raman, R. Mohanraman, F. C. Chou, Y. Y. Chen, C. H. Lee, F. C. Chang and C. W. Chu, *Sol. Energy Mater Sol. Cells,* **121**, 35 (2014).

15. Q. Wei, J. Chen, P. Ding, B. Shen, J. Yin, F. Xu, Y. Xia and Z. Liu, *ACS Appl. Mater. Interfaces*, **27**, 21527 (2018).

16. A. D. Bailey, A. R. Baru, K. K. Tasche and R. S. Mohan, *Tetrahedron Lett.*, **49**, 21527 (2008).

17. N. Soltanzadeh and A. Morsali, *Ultrason Sonochem.*, **17**, 21527 (2010).

18. X. Chang, J. Huang, Q. Tan, M. Wang, G. Ji, S. Deng and G. Yu, *Catal. Commun.* **10**, 1957 (2009).

19. Y. Wang, K. Deng and L. Zhang, *J. Phys. Chem. C*, **115**, 14300 (2011).

20. A. C. Mera, Y. Moreno, J. Y. Pivan, O. Pena and H. D. Mansilla, *J. Photochem. Photobiol*, **289**, 7 (2014).

21. Y. Huang, H. Li, M. S. Balogun, W. Liu, Y. Tong, X. Lu and H. Ji, *ACS Appl. Mater. Interfaces* **6**, 22920 (2014).

22. Y. Huang, H. Li, W. Fan, F. Zhao, W. Qiu, H. B. Ji and Y. Tong, *ACS Appl. Mater. Interfaces*, **8**, 27859 (2016).

23. X. Shi, X. Chen, X. Chen, S. Zhou and S. Lou, *Mater. Lett.*, **68**, 296 (2012).

24. P. Q. Wang, Y. Bai, J. Y. Liu, Z. Fan and Y. Q. Hu, *IET Micro & Nano Letters*, **8**, 296 (2013).

25. D. Shu, J. Wu, Y. Gong, S. Li, L. Hu, Y. Yang and C. He, *Catal. Today*, **224**, 13 (2014).

26. J. Han, G. Zhu, M. Hojamberdiev, J. Peng, X. Zhang, Y. Liu, B. Ge and P. Liu, *New J. Chem.*, **39**, 1874 (2015).

27. L. Ye, J. Chen, L. Tian, J. Liu, T. Peng, K. Deng and L. Zan, *Appl. Catal. B,* **130–131**, 1 (2013).

28. P. Kwolek and K. Szaciłowski, *Electrochim. Acta*, **104**, 448 (2013).

29. J. M. M. Zamora, A. M. D. L. Cruz and E. L. Cuéllar, *J. Taiwan Inst. Chem. Engg.*, **75**, 307 (2017).

30. M. S. Kandanapitiye, M. Gao, J. Molter, C. A. Flask and S. D. Huang, *Inorg. Chem.* **53**, 10189 (2014).

31. I. D. Sharma, G. K. Tripathi, V. K. Sharma, S. N. Tripathi, R. Kurchania, C. Kant, A. K. Sharma and K. K. Saini, *Cogent Chem.*, 1 (2015).

32. Y. Long, Y. Wang, D. Zhang, P. Ju and Y. Sun, *J. Colloid Interface Sci.,* **481**, 47 (2016).

33. V. Mahmoodi, A. Ahmadpour, T. R. Bastami and M. T. H. Mousavian, *Photochem. Photobiol.,* **94**, 4 (2018).

34. M. E. Kazyrevich, M. V. Malashchonak, A. V. Mazanik, E. A. Streltsov, A. I. Kulak and C. Bhattacharya, *Electrochim. Acta,* **190**, 612 (2016).

35. S. Vadivel, B. Saravanakumar, M. Kumaravel, D. Maruthamani, N. Balasubramanian, A. Manikandan, G. Ramadoss, B. Paul and S. Hariganesh, *Mater. Lett.*, **210**, 109 (2018)

36. A. Banik, E. W. Bohannan, J. A. Switzer, *Chem. Mater.*, **32**, 19 (2020).

37. K. J. McDonald and K. S. Choi, *Energy. Environ. Sci.*, **5**, 8553 (2012).

38. J. Gan, B. B. Rajeeva, Z. Wu, D. Penley and Y. Zheng, *Electrochim. Acta,* **219**, 20 (2016).

39. P. Sengupta, S. Shinde, P. Majumdar, M. Löffler, P. Datta and S. Patra, *J. Electrochem. Soc.*, **167**, 047513 (2020).

40. E. Sandnes, M. E. Williams, U. Bertocci, M. D. Vaudin and G. R. Stafford, *Electrochim. Acta*, **52**, 6221 (2007).

41. A. R. Rajamani, S. Jothi, M. D. Kumar, S. Srikaanth, M. K. Singh, G. O. Irurueta, D. Ramasamy, M. Datta and M. Rangarajan, *J. Phys. Chem. C*, **120**, 22398 (2016).

42. A. R. Rajamani, U. B. R. Ragula, N. K. Kothurkar, M. Rangarajan, *CrystEngComm*, **16**, 2032 (2014).

43. E. I. Rogers, D. S. Silvester, L. Aldous, C. Hardacre and R. G. Compton, *J. Phys. Chem. C*, **112**, 6551 (2008).

44. I. Lengyel, I. R. Epstein and K. Kusth, *Inorg. Chem.*, **32**, 5880 (1993).

45. Tooth, B. The Hydrothermal Chemistry of Bismuth and The Liquid Bismuth Collector Model. Ph.D. thesis, University of Adelaide, (https://digital.library.adelaide.edu.au/dspace/bitstream/2440/83112/8/02whole.pdf), (2013).

46. C. C. Pye, C. M. Gunasekara and W. W. Rudolph, *Can. J. Chem*, **85**, 945 (2007).

47. D. Knetsch and W. L. Groeneveld, *Inorganica Chim. Acta*, **7**, 81 (1973).

48. D. Knetsch and W. L. Groeneveld, *Rec. Trav. Chim. Pays Bas*, **92**, 855 (1973).

49. M. D. Prasad, L. D. V. Sangani, S. K. Batabyal and M. G. Krishna, *CrystEngComm*, **20**, 5880 (2018).

50. M. D. Prasad, M. G. Krishna and S. K. Batabyal, *ACS Appl. Nano Mater*., **4**, 1252 (2021).

51. A. Osol and C. C. Pines, *J. Am. Pharm. Assoc.*, **XLI**, 634 (1952).

52. M.D. Levi, H. Gizbar, E. Lancry, Y. Gofer, E. Levi and D. Aurbach, *J. Electroanal. Chem*, **569**, 211 (2004).

53. M. Sajjad, N. Singh and J. A. Larsson, *AIP Advances* **10**, 075309 (2020).

54. D. Kato, K. Hongo, R. Maezono, M. Higashi, H. Kunioku, M. Yabuuchi, H. Suzuki, H. Okajima, C. Zhong, K. Nakano, R. Abe and H. Kageyama, *J. Am. Chem. Soc.*, **139**, 18725 (2017).

55. L. Liu, W. Liu, X. Zhao, D. Chen, R. Cai, W. Yang, S. Komarneni and D. Yang, *ACS Appl. Mater. Interfaces*,**6**, 16082 (2014).

56. Y. Xiong, B. Dang, C. Wang, H. Wang, S. Zhang, Q. Sun and X. Xu, *ACS Appl. Mater. Interfaces*,**9**, 20554 (2017).

57. L. Zhang, A. A. S. Goncalves, B. Jiang and M. Jaroniec, *chemsuschem*, **11,** 1486 (2018).

58. W. E. Morgan, W. J. Stec and J. R. V. Wazer, *Inorg. Chem.*, **12**, 627 (1973).

59. X. Zhang and L. Zhang, *J. Phys. Chem. C*, **114**, 18198 (2010).

60. J. Cao, B. Xu, H. Lin, B. Luo and S. Chen, *Dalton Trans*., **41**, 11482 (2012).

61. S. Han, J. Li, K. Yang and J. Lin, *Chin. J. Catal.*, **36**, 2119 (2015).

62. Y. R. Jiang, S. Y. Chou, J. L. Chang, S. T. Huang, H. P. Lin, C. C. Chen, *RSC Adv.*, **5,** 30851 (2015).

63. A. C. Mera, Y. Mareno, D. Contreras, N. Escalona, M. F. Melendrez, R. V. Mangalaraja, H. D. Mansilla, *Solid State Sci.*, **63**, 84 (2017).

64. N. J. Podraza, W. Qiu, B. B. Hinojosa, H. Xu, M. A. Motyka, S. R. Phillpot, J. E. Baciak, S. T. McKinstry and J. C. Nino, J. Appl. Phys., 114, 033110-1 (2013).